PREOPERATIVE SIMULATION FOR MICROVASCULAR DECOMPRESSION IN PATIENTS WITH IDIOPATHIC TRIGEMINAL NEURALGIA: VISUALIZATION WITH THREE-DIMENSIONAL MAGNETIC RESONANCE CISTERNOGRAM AND ANGIOGRAM FUSION IMAGING

Toru Satoh, M.D.

Department of Neurological Surgery, Ryofukai Satoh Neurosurgical Hospital, Hiroshima, Japan

Keisuke Onoda, M.D.

Department of Neurological Surgery, Okayama University, Graduate School of Medicine, Dentistry and Pharmaceutical Sciences, Okayama, Japan

Isao Date, M.D.

Department of Neurological Surgery, Okayama University, Graduate School of Medicine, Dentistry and Pharmaceutical Sciences, Okayama, Japan

Reprint requests:
Toru Satoh, M.D., Department of Neurological Surgery, Ryofukai Satoh Neurosurgical Hospital, Matsunaga, 5–23–23, Fukuyama, Hiroshima, 729–0104, Japan.
Email: ucsfbtrc@urban.ne.jp

Received, May 23, 2006.
Accepted, August 23, 2006.

OBJECTIVE: Precise assessment of the complex nerve-vessel relationship at the root entry zone of the trigeminal nerve is useful for planning microvascular decompression in patients with idiopathic trigeminal neuralgia. We have applied a fusion imaging technique of three-dimensional (3-D) magnetic resonance cisternography and co-registered 3-D magnetic resonance angiography (MRA) that allows virtual reality for the preoperative simulation of the neurovascular conflict at the trigeminal nerve root entry zone.

METHODS: Fusion images of 3-D magnetic resonance cisternograms and angiograms were reconstructed by a perspective volume-rendering algorithm from the volumetric data sets of magnetic resonance cisternography, obtained by a T2-weighted 3-D fast spin echo sequence, and co-registered MRA, by a 3-D time-of-flight sequence. Consecutive series of 12 patients with idiopathic trigeminal neuralgia were studied with fusion 3-D magnetic resonance cisternogram and MRA in the preoperative assessment for the microvascular decompression of the affected trigeminal nerve.

RESULTS: The complex anatomical relationship of the offending vessels to the trigeminal nerve root entry zone was depicted on the fusion 3-D magnetic resonance cisternogram and MRA. The presence of offending vessels and compressive site of neurovascular conflict was assessed from the various viewpoints within the cistern and was presumed by the preoperative simulation through the surgical access (surgeon's-eye view). The blinded surgical trajectory was discerned by the virtual image through the opposite direction projected from above (bird's-eye view). The 3-D visualization of the nerve-vessel relationship with fusion images was consistent with the intraoperative trajectory and findings.

CONCLUSION: Fusion imaging of 3-D magnetic resonance cisternogram and MRA may prove a useful adjunct for the diagnosis and decision-making process to execute the microvascular decompression in patients with idiopathic trigeminal neuralgia.

KEY WORDS: Cranial nerve, Magnetic resonance cisternography, Neurovascular conflict, Trigeminal neuralgia

Neurosurgery 60:104-114, 2007 DOI: 10.1227/01.NEU.0000249213.34838.C9 www.neurosurgery-online.com

Idiopathic trigeminal neuralgia (ITN) is a neurovascular compression syndrome caused by hyperactive dysfunction of the cranial nerves and is characterized by paroxysmal, electric, lancinating pains, and a variety of sensory experiences (2, 4, 12, 13). In most instances, mechanical compression of the trigeminal nerve at the root entry zone (REZ) by the aberrant artery and/or vein causes the symptoms. The microvascular decompression (MVD) of the affected trigeminal nerve via the lateral suboccipital approach is widely performed to treat the patients with ITN, resulting in an improvement of symptoms and long-term relief in the majority of cases (9, 12, 13, 18, 25).

For assessment of the neurovascular conflict in patients with ITN, it is important to depict offending vessels at the REZ of the trigeminal

nerve. With recent advances in magnetic resonance imaging (MRI) technology (1–3, 5–8, 14–17, 19–24, 26–28), magnetic resonance cisternography and magnetic resonance angiography (MRA) can depict the fine structures of cranial nerves, arteries, and veins within the cerebellopontine angle cistern in conjunction with the adjacent brain parenchyma, dura mater, and cranial base bones. The offending vessels causing the neurovascular compression can be seen on the source image of volumetric data. Because these data display the anatomic elements in a two-dimensional fashion, a physician may discern the relationships of the nerve-vessel complex at the trigeminal nerve REZ more easily in three-dimensional (3-D) displays.

In this study, we used the fusion imaging technique of 3-D magnetic resonance cisternogram and 3-D MRA (22–24) for 3-D visualization of the anatomic relationship of the neurovascular conflict in patients with ITN. The 3-D magnetic resonance cisternogram was reconstructed from the volumetric data of the magnetic resonance cisternography, obtained by T2-weighted 3-D fast spin echo (FSE) sequence and 3-D magnetic resonance angiogram from MRA by 3-D time-of-flight (TOF) spoiled gradient recalled (SPGR) sequence, with or without administration of contrast medium in the steady-state. By using the workstation with computer medical visualization software, images of black blood T2-weighted FSE magnetic resonance cisternogram and bright blood TOF, SPGR magnetic resonance angiogram were co-registered and composed in a single 3-D image.

With a fusion 3-D magnetic resonance cisternogram/angiogram, the presence of offending vessels and the site of neurovascular compression were assessed preoperatively and visualized in 3-D display from various viewpoints in the cerebellopontine angle cistern. Preoperative simulation images through the surgical access (surgeon's-eye view) were reconstructed and compared with the intraoperative trajectory and findings. In addition, the blinded surgical trajectory was discerned by the virtual image through the opposite direction projected from above (bird's-eye view). Usefulness and accuracy of the fusion image of 3-D magnetic resonance cisternogram/angiogram in the preoperative assessment and simulation to execute a MVD for ITN were discussed with some comments on the imaging technique and the significance of the fusion magnetic resonance findings.

MATERIALS AND METHODS

Patients and Clinical Data

A consecutive series of 12 patients with ITN, introduced by the physicians as a result of resistance to medical treatment, who underwent MVD surgery at our hospital between January 2005 and April 2006 were included in this study (*Table 1*). The patients' ages ranged from 36 to 80 years old (mean, 67.8 $\pm$12.2 yr; five men, seven women). Five patients were treated on the right side, and seven patients were treated on the left side. All patients underwent magnetic resonance cisternography and MRA preoperatively and received MVD via the lateral suboccipital approach.

Magnetic Resonance Cisternography Data Acquisition

Magnetic resonance cisternography was performed with a clinical magnetic resonance imager (Signa HiSpeed 1.0T; General Electric Healthcare, Milwaukee, WI), using a quadrature head coil and a T2-weighted 3-D FSE sequence. We used the following parameters: repetition time (TR)/echo time (TE) 4000/160; number of excitations, one; echo train length, 128; bandwidth, 15.63 KHz; matrix, 256 $\times$ 256; section thickness, 0.6 mm; section interval, 0.6 mm; field of view, 16 cm; voxel size, 0.625 $\times$ 0.625 $\times$ 0.6 mm; and total imaging time, 13 minutes

TABLE 1. Clinical features of 12 cases of idiopathic trigeminal neuralgia treated with microvascular decompression[a]

Patient no.	Age (yr)/sex	Side	Location of neuralgia	Offending vessels on 3-D images	Compressed site on 3-D images	Offending vessels at surgery	Outcome
1	59/F	Rt	III	SCA-t, c	Superior	SCA-t, c	Excellent
2	76M	Rt	I>II>III	SCA-t, r, c	Superomedial	SCA-t, r, c	Excellent
3	80/F	Rt	II	SCA-r, c	Superior	SCA-r, c	Excellent
4	71/M	Lt	III	SCA-t	Superomedial	SCA-t	Excellent
5	73/F	Lt	III	SCA-r	Superior	SCA-r	Excellent
6	72/M	Rt	I>II>III	SCA-r/SPV	Superior/inferior	SCA-r/SPV	Excellent
7	73/F	Lt	III	SCA-r/SPV	Superomedial/inferior	SCA-r	Excellent
8	74/F	Rt	I>II	PICA/VA	Inferomedial	PICA/VA	Excellent
9	72/M	Lt	II<I	AICA	Inferomedial	AICA	Excellent
10	73/F	Lt	II<III	SCA-t, r, c	Superomedial	SCA-t, r, c	Excellent
11	55/M	Lt	II	SCA-r	Superomedial	SCA-r	Excellent
12	36/F	Lt	III	SCA-t, c	Superomedial	SCA-t, c	Excellent

[a] 3-D, three-dimensional; Rt, right; Lt, left. Offending vessels: SCA-t, trunk of superior cerebellar artery; SCA-c, caudal branch of superior cerebellar artery; SCA-r, rostral branch of superior cerebellar artery; SPV, superior petrosal vein; VA, vertebral artery; PICA, posterior inferior cerebellar artery; AICA, anterior inferior cerebellar artery.

and 23 seconds. A total of 96 continuous source axial volumetric data were acquired. Data were transferred to a commercially available independent workstation (M900 Quadra; AMIN, Tokyo, Japan) with computer medical visualization software (Ziosoft, Tokyo, Japan).

The imaging technique for reconstruction of 3-D magnetic resonance cisternogram was described previously (22–24). Briefly, data of magnetic resonance cisternography were processed into the 3-D volume-rendering data set (96 data points) in 9 seconds. The images were rendered from the data set in 11 seconds using a perspective volume-rendering algorithm. To assess the range of signal intensity assigned to the certain anatomic elements, we used histograms (arbitrary unit distribution) of the magnetic resonance signal intensity along the line drawn on the source axial magnetic resonance cistenogram. The histograms revealed that the arteries, veins, and dura mater showed profoundly low signal intensity (50–150), cranial nerves and juxtacisternal brain parenchyma showed moderately low signal intensity (250–300), and surrounding cerebrospinal fluid showed profoundly high signal intensity (500–750). To visualize the margin of vessels, cranial nerves, and brainstem in a 3-D fashion, we selected the entire area that was hypointense relative to cerebrospinal fluid from the opacity chart of signal-intensity distribution (the arbitrary signal intensity unit in the *x*-axis and the opacity percent in the *y*-axis), using a function of declining curve. The threshold value of this curve was adjusted according to each individual signal intensity distribution pattern with a threshold range of 330 to 430 (100% opacity level), declining from 350 to 450 (0% opacity level; width 20), and color-rendered in blue. By shifting the opacity curve to the left and right, we could remove the cerebrospinal fluid and find the best visualization threshold for the intracisternal nerve and vessels in conjunction with the juxtacisternal brainstem at the maximum threshold value (350–450) of signal intensity. 3-D magnetic resonance cisternograms were projected and inspected from various viewpoints within the cistern with a visual angle (projection angle with the method of perspective volume-rendering algorithm) of 90 degrees. With this imaging technique, the 3-D magnetic resonance cisternogram depicted the spatial relationship of the intra- and juxtacisternal anatomic elements comprising of the neurovascular compression in patients with ITN.

MRA Data Acquisition

MRA was performed with the same scan baseline, and data were obtained using a 3-D TOF, SPGR sequence. We used the following protocol: TR/TE, 35/3.9 to 4.1; number of excitations, two; flip angle, 20 degrees; matrix, 192 × 128; section thickness, 1.2 mm; section interval, 0.6 mm; field of view, 16 cm; voxel size, 0.83 × 1.25 × 1.2 mm; no magnetization transfer contrast; zero-fill interpolation processing two times; 120 sections in total (two slabs); overlap of eight sections; and total imaging time, 8 minutes 49 seconds. A total of 104 continuous source axial volumetric data were obtained. Following this non-contrasted MRA, a steady-state contrast-enhanced MRA was repeatedly performed and started 3 minutes after 0.1 mmol/kg intravenous administration of meglumine gadopentate (Magnevist; Schering Japan Co., Tokyo, Japan) via the antecubital vein.

The volumetric data of non-contrasted and contrast-enhanced MRA were transferred to the same workstation and were interpolated every 0.6 mm, then processed into the 3-D volume-rendering data set (207 data points). The 3-D magnetic resonance angiogram was rendered with a perspective volume-rendering algorithm by using an increasing curve starting with a threshold of 160 to 180 (0% opacity level) and up to 180 to 200 (100% opacity level; width, 20), with a visual angle of 90 degrees, and color-rendered in red. The non-contrasted 3-D magnetic resonance angiogram showed the spatial architecture of the arteries and large veins with high signal intensity. The contrast-enhanced 3-D magnetic resonance angiogram depicted those vessels with enhancement; moreover, small branching arteries, tributary veins, and venous sinuses were depicted as structures with high signal intensity.

Reconstruction of Fusion 3-D Magnetic Resonance Cisternogram/Angiogram

A fusion image of 3-D magnetic resonance cisternogram/angiogram was reconstructed on a workstation by co-registering the 3-D magnetic resonance cisternogram and its coordinated 3-D magnetic resonance angiogram in a single 3-D image, according to the imaging technique as described previously (22–24); each individual image was rendered from each volume-rendering data set. To emphasize the vascular components, we used a MRA-weighted fusion image by compositing 3-D magnetic resonance cisternogram (opacity level 15%, in blue) and 3-D magnetic resonance angiogram (opacity level 100%, in red). Alternatively, we used a boundary imaging technique of 3-D magnetic resonance cisternogram (21, 23) and rendered with a perspective volume-rendering algorithm by using a spiked peak curve with a threshold of 330 to 450 (opacity level 100%; width 40, in blue) and a square curve with 330 to 450 (opacity level 5%; width 330–450, in blue). The boundary image of 3-D magnetic resonance cisternogram sharply depicted the border of the intra- and juxtacisternal structures as a series of rings (opacity level 100%, in blue), so that the underlying 3-D magnetic resonance angiogram (opacity level 100%, in red) could be visualized directly through the spaces between the rings.

Using reconstruction parameters of the function curves saved on the workstation, we instantly reproduced standard 3-D magnetic resonance cisternogram, 3-D magnetic resonance angiogram, fusion 3-D magnetic resonance cisternogram/angiogram, and boundary images. The simulated images of the operative field through similar surgical access were feasibly reconstructed for the different clinical cases; however, certain adjustments of the threshold range to refine the contours of the objects and minor change in projections from different viewpoints were needed in each individual case. The overall average time required to reconstruct those images was approximately 30 to 50 seconds per image after magnetic resonance scanning.

With a boundary fusion image of 3-D magnetic resonance cisternogram/angiogram, the 3-D relationship of the nerve-vessel complex was preoperatively assessed from the various viewpoints in the cerebellopontine angle cistern. The simulated image, through the surgical approach (surgeon's-eye view), and the virtual image, through the opposite direction projected from above (bird's-eye view), were compared with the intraoperative trajectory and findings, which were recorded with digital video tape recording. We determined the imaging findings of the neurovascular contact before MVD surgery and discussed the similarity between the imaging and intraoperative findings postoperatively. By reviewing the digital video tape recording of MVD surgery, we reproduced and reconstructed virtual reality with the dynamic animation display of 3-D images comparative to the actual operative trajectory and operative field again.

RESULTS

On the 3-D magnetic resonance cisternograms, the anatomic elements in the cerebellopontine angle cistern, including the nerve-vessel complex at the REZ of the trigeminal nerve, were depicted simultaneously. The trigeminal nerve was identified on the basis of the course from the orifice of Meckel's cave towards the rootlet at the brainstem. The arteries were identified by tracing the vessels to their origin in the basilar artery and vertebral artery (VA) and the tributaries of the superior petrosal vein (SPV) to a larger vein and the superior petrosal venous sinus. The arteries showed profoundly low signal intensity and were distinguishable from the cranial nerves and brain parenchyma with moderately low signal intensity but were not usually differentiated from the veins.

Meanwhile, non-contrasted 3-D magnetic resonance angiogram showed the arteries and large veins with high signal intensity. The contrast-enhanced 3-D magnetic resonance angiogram depicted those vessels with enhancement and small arteries, including rostral and caudal branches of the superior cerebellar artery (SCA) and tributaries of SPV with high signal intensity. Those vessels were strongly contrasted to the adjacent nerve and brainstem at the trigeminal nerve REZ with moderately low signal intensity. In addition, to trace the vessels to the parent vessels, comparison of non-contrasted and contrast-enhanced magnetic resonance angiograms provided additional information to distinguish the vascular structure as an artery and a vein.

While the boundary fusion 3-D magnetic resonance cisternogram/angiogram depicted the complicated intra- and juxtacisternal structures in a single 3-D display, including nerve, vessels, brainstem, and cranial base bones, the vascular components of the 3-D magnetic resonance cisternogram can be discriminated by referencing the overlapped 3-D magnetic resonance angiogram. The contact between the offending vessels and the trigeminal nerve at the REZ could be visualized and represented from various viewpoints in the cerebellopontine angle cistern, including a simulated surgical approach.

Offending vessels at the REZ of the trigeminal nerve were as follows: SCA 8 (SCA-trunk, 5; SCA-rostral branch, 7; SCA-caudal branch, 5), SCA (SCA-rostral branch) and SPV 2, posterior inferior cerebellar artery (PICA), VA 1, and anterior inferior cerebellar artery (AICA) 1. These findings were confirmed by intraoperative studies in 11 out of 12 cases (*Table 1*). Compressive sites of the offending vessels at the REZ of the trigeminal nerve were categorized as superior to the nerve in three, superomedial in five, superior/inferior in one, superomedial/inferior in one, and inferomedial in two (*Table 1*). Outcome of the MVD surgery was excellent in all patients, and symptom relief was complete immediately after surgery or after a few days without any complications.

ILLUSTRATIVE CASES

Patient 3

(see video at web site)

An 80-year-old woman (Patient 3; *Table 1; Fig. 1*) received MVD because of insufficient medical control of the right ITN for 15 years and aggravation for 3 months. The source contrast-enhanced magnetic resonance angiogram (*Fig. 1A*), projected superoinferiorly, showed the right SCA and veins around the course of the right trigeminal nerve. The source magnetic resonance cisternogram (*Fig. 1B*), projected superoinferiorly, showed the right SCA crossing the right trigeminal nerve. The operative photograph (*Fig. 1C*) showed the REZ of the right trigeminal nerve compressed by the right SCA tributaries. Preoperative contrast-enhanced 3-D magnetic resonance angiogram (*Fig. 1D*), co-registered 3-D magnetic resonance cisternogram (*Fig. 1E*), and boundary fusion images of 3-D magnetic resonance cisternogram/angiogram (*Fig. 1F*) projected right posterolaterally as indicated by an arrowhead in *Figure 1B* and the view-position box at the right corner and depicted the preoperative simulation through the surgical access (surgeon's-eye view). The spatial relationship of the offending right SCA, surrounding SPV, AICA, and the right trigeminal nerve REZ, was clearly depicted. The trigeminal nerve was compressed (empty arrowhead) at the peripheral one-third of the cistern by the right SCA at its bifurcation into the rostral and caudal branches from the superomedial direction. The 3-D visualization of the nerve-vessel relationship was consistent with the intraoperative trajectory and findings as shown in *Figure 1C*. Additionally, the contrast-enhanced 3-D magnetic resonance angiogram (*Fig. 1G*), co-registered 3-D magnetic resonance cisternogram (*Fig. 1H*), and boundary fusion 3-D magnetic resonance cisternogram/angiogram (*Fig. 1I*), in the opposite direction to the surgical access and projected from above (bird's-eye view), showed the architecture of the right SCA and its rostral and caudal branches along with the entire shape of the right trigeminal nerve within the cistern and confirmed the spatial relationship of the offending vessels and the trigeminal nerve at the REZ. By reviewing the MVD digital VTR, we constructed virtual reality usually with the dynamic animation display of 3-D images comparable to the actual operative trajectory and operative field.

Patient 11

(see video at web site)

A 55-year-old man (Patient 11; *Table 1, Fig. 2*) received MVD because of a 3-year history of left TN and deterioration in the 3 months as a result of insufficient medical control. The selected minimum intensity

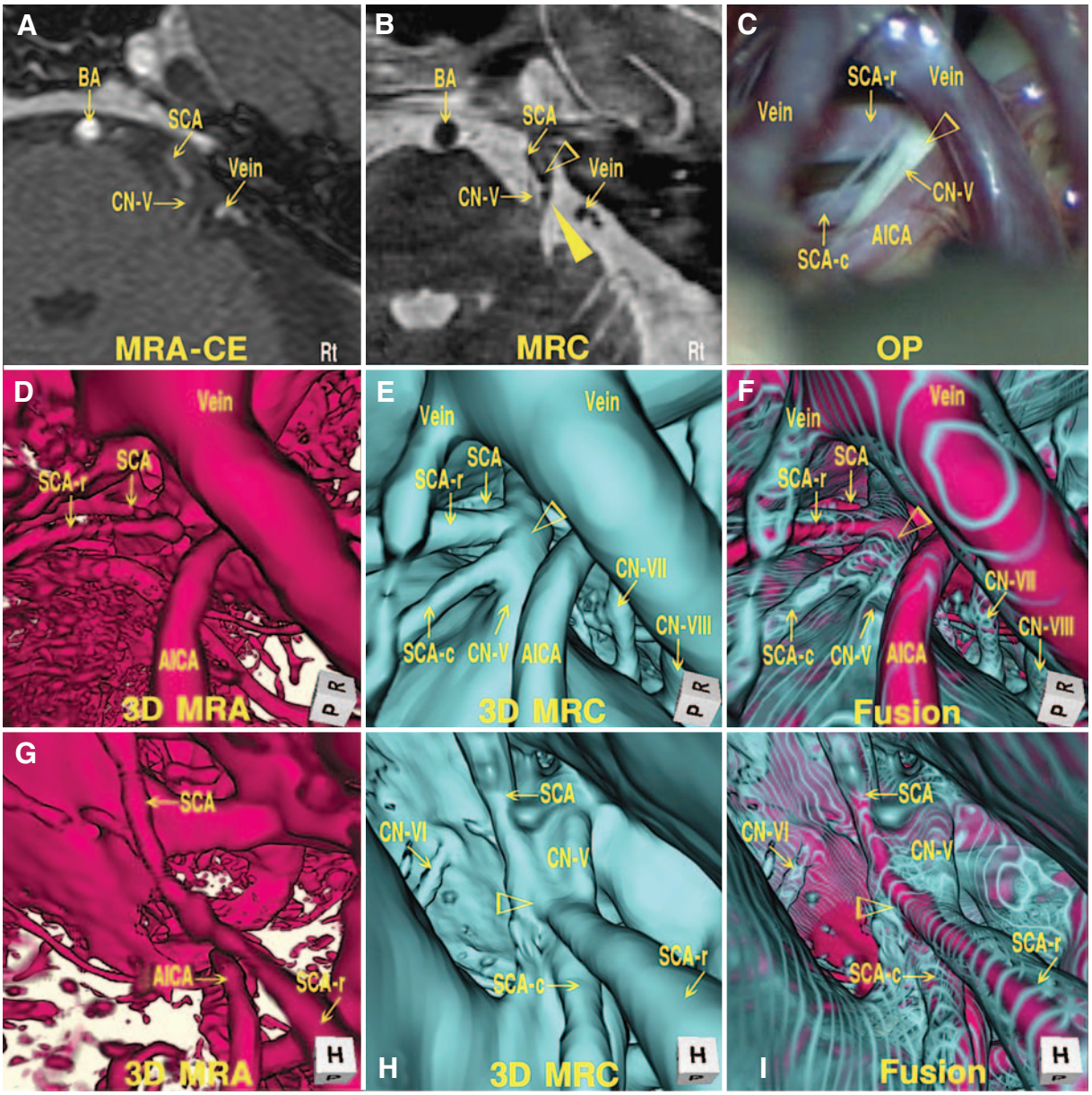

FIGURE 1. *Patient 3 (Table 1).* A, *source contrast-enhanced MRA, projected superoinferiorly, showing the right superior cerebellar artery and superior petrosal veins around the course of the right trigeminal nerve.* B, *source magnetic resonance cisternogram, projected superoinferiorly, showing the right superior cerebellar artery crossing the right trigeminal nerve.* Arrowheads *indicate the viewing position for preoperative simulation images in* D, E, *and* F. C, *operative photograph showing the root entry zone of the right trigeminal nerve, compressed* (empty arrowhead) *by the rostral and caudal branches of the right superior cerebellar artery. Contrast-enhanced 3-D MRA* (D), *co-registered 3-D magnetic resonance cisternogram* (E), *and fusion 3-D magnetic resonance cisternogram/angiogram* (F) *projected right posterolaterally, as indicated by an* arrowhead *in* B *and the* view-position box *at the right corner, depicting the preoperative simulation through the surgical access (surgeon's-eye view). The spatial relationship of the offending right superior cerebellar artery and the trigeminal nerve was depicted in conjunction with the surrounding superior petrosal veins and anterior inferior cerebellar artery. The trigeminal nerve was compressed by the right superior cerebellar artery at its bifurcation (SCA-trunk, SCA-rostral, and SCA-caudal branches) from the superomedial direction* (empty arrowhead). *Contrast-enhanced 3-D MRA* (G), *co-registered 3-D MR cisternogram* (H), *and fusion 3-D magnetic resonance cisternogram/angiogram* (I), *opposite direction to the surgical access and projected from above (bird's-eye view), showing the architecture of the right superior cerebellar artery and its rostral and caudal tributaries and the entire shape of the right trigeminal nerve within the cistern.* 3D, *three-dimensional;* AICA, *anterior inferior cerebellar artery;* BA, *basilar artery;* CN-V, *Cranial Nerve V;* CN-VI, *Cranial Nerve VI;* CN-VII, *Cranial Nerve VII;* CN-VIII, *Cranial Nerve VIII;* MRA-CE, *contrast-enhanced magnetic resonance angiography;* MRC, *magnetic resonance cisternogram;* OP, *operative photograph;* SCA, *superior cerebellar artery;* SCA-c, *superior cerebellar artery, caudal branches;* SCA-r, *superior cerebellar artery, rostral branches.*

projection image of the magnetic resonance cisternography (*Fig. 2A*) projected superoinferiorly and showed the left SCA crossing the left trigeminal nerve at the REZ. Preoperative 3-D magnetic resonance cisternogram (*Fig. 2B*) and fusion 3-D magnetic resonance cisternogram/angiogram (*Fig. 2C*) projected left inferoposterolaterally, as indicated by an arrowhead in *Figure 2A* and the view-position box at the right corner, and showed the preoperative simulation through the surgical access (surgeon's-eye view). The spatial relationship of the offending left SCA and the left trigeminal nerve at the REZ was depicted in conjunction with AICA and veins (see video at web site). The trigeminal nerve was compressed (empty arrowhead) at the peripheral two-thirds of the cistern by the rostral branch of the left SCA from a superior direction. The 3-D visualization of the nerve-vessel relationship was consistent with the intraoperative trajectory and findings (*Fig. 2D*). The 3-D magnetic resonance cisternogram (*Fig. 2E*) and fusion 3-D magnetic resonance cisternogram/angiogram (*Figure 2F*) in the opposite direction to the surgical access and projected from above (bird's-eye view), visualized the spatial architecture of the left SCA and its rostral and caudal tributaries in relation to the entire shape of the right trigeminal nerve within the cistern from the orifice in Meckel's cave to the rootlet at the brainstem. With the preoperative imaging analysis previously mentioned, the offending vessel was confirmed to be the rostral branch of the left SCA and compressed site at the superior aspect of the left trigeminal nerve within the cistern and near Meckel's cave. For the virtual reality of the actual operative simulation, we reconstructed the dynamic animation display of 3-D images.

DISCUSSION

The neurovascular conflict in patients with ITN is caused by the vessels compressing the REZ of the affected trigeminal nerve (2, 4, 12, 13, 25). The offending vessels are either arteries, including SCA, AICA, PICA, BA, and VA, or tributaries of SPV draining into the superior petrosal sinus (12, 18). The most common single offending vessel is the SCA and its rostral and caudal branches, but the vein alone, or in combination with the artery, rarely contributes to the compression. Regarding the diagnosis and the decision-making process to forego a MVD for ITN, it may be useful to depict the presence of the offending vessels and compressive site of the neurovascular conflict before surgery. In addition, the virtual reality of the preoperative 3-D simulation images with dynamic animation display through the surgical access (surgeon's-eye view) may be helpful to understand the spatial anatomic relationship of the nerve-vessel complex at the REZ of the trigeminal nerve.

MRI for Trigeminal Neuralgia

Recent advances in MRI technology (1–3, 5–8, 14–17, 19–24, 26–28), including magnetic resonance cisternography and MRA, provide the volumetric data of the fine anatomic elements within the cerebellopontine angle cistern, in conjunction with the surrounding brain parenchyma, dura mater, and cranial base bones. The anatomic relationship of the offending vessels to the trigeminal nerve at the REZ can be viewed on the volumetric data of the source MRI.

The magnetic resonance cisternography represents the vascular structures, cranial nerves, and brain parenchyma with low signal intensities, so that the space-occupying intra- and juxtacisternal structures are well demarcated by the hyperintense adjacent subarachnoid cerebrospinal fluid. On the source images of volumetric data obtained by the constructive interference in steady-state (1, 16, 17, 27, 28), fast imaging using steady-state acquisition (5), true fast inflow with steady-state acquisition (1), and balanced fast field echo (26), the signal intensities of the cranial nerves, vessels, and brain parenchyma are similar. Therefore, it is difficult to differentiate the boundary of each anatomic element. In addition, because the images show a composite nature of gradient echo and spin echo sequences, a relatively hyperintense area related to susceptibility and flow artifacts unexpectedly appeared within the large vessels (16, 26). It may be required to judge the shape and contents of the vascular components. In contrast, magnetic resonance cisternography obtained by T2-weighted 3-D FSE (14, 15, 19–24) or 3-D fast asymmetric spin echo (16) sequences, with fine adjustment of TR/TE (TR, 4000 ms; TE, 160ms in the present study) can depict the vascular structures as complete flow voids with profoundly low signal intensity (black blood), the cranial nerves and brain parenchyma, with moderately low signal intensity, and the cerebrospinal fluid, with profoundly high signal intensity. These features may be useful to distinguish the boundary of vascular structures from the cranial nerves and the adjacent brainstem.

The MRA obtained by the 3-D TOF, SPGR sequence is a T1-weighted gradient echo image. Therefore, the cranial nerves and brain parenchyma are depicted with relatively low signal intensity and the vascular structures with profoundly high signal intensity (bright blood) (1–3, 17, 21–24, 27). The arteries and large veins near the REZ of the trigeminal nerve, with fast flow velocity, are clearly visualized in contrast to the adjacent brainstem and cerebellum. The steady-state contrast-enhanced MRA (2, 11), obtained by the 3-D TOF, SPGR sequence with an intravenous administration of contrast medium, can be enhanced to depict vessels with relatively slow flow velocity because of the T1-shortening effect of intravascular paramagnetic agents. The rostral and caudal branches and distal portions of SCA are represented more clearly than those with conventional non-contrasted MRA, in conjunction with enhancement of SPV and venous sinuses. However, vascular structures represented by 3-D TOF, SPGR sequence with or without contrast-enhancement do not indicate the pure luminal morphology, as shown by digital angiography and computed tomographic angiography. The MRA represents the intravascular flow information caused by inflow effect related mainly to the peak flow velocity within the vessels with or without T1-shortening effect (21–24). Therefore, assessment of the vessel-nerve relationship may be possible on the SPGR image, but it may be difficult to define the fine contact of an offending vessel to the trigeminal nerve at the REZ.

3-D Visualization of Neurovascular Conflict

Although magnetic resonance cisternography and MRA provide the fine volumetric data of the complicated nerve-

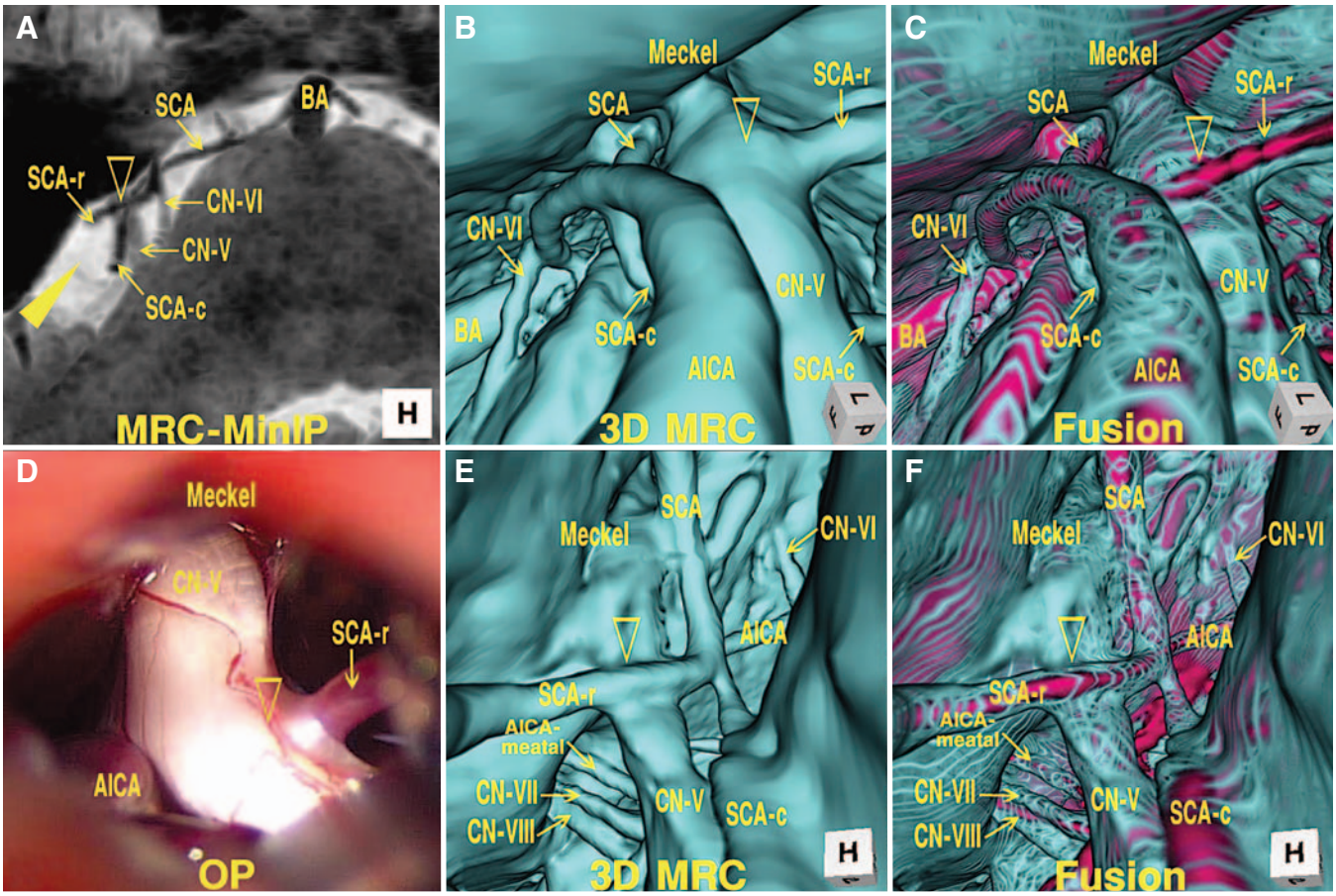

FIGURE 2. *Patient 11 (Table 1).* A, *selected minimum intensity projection image of the magnetic resonance cisternography projects superoinferiorly and shows the left superior cerebellar artery crossing the left trigeminal nerve.* Arrowheads *indicate the viewing position for preoperative simulation images in* B *and* C. *3-D magnetic resonance cisternogram* (B) *and fusion 3-D magnetic resonance cisternogram/angiogram* (C) *project left inferoposterolaterally, as indicated by an* arrowhead *in* A *and the* view-position box, *at the right corner, and depict the preoperative simulation through the surgical access (surgeon's-eye view). The spatial relationship of the offending right superior cerebellar artery and the trigeminal nerve was shown in relation to the anterior inferior cerebellar artery and superior petrosal veins. The left trigeminal nerve was compressed at the peripheral two- thirds of the cistern by the rostral branch of the left SCA from the superior direction* (empty arrowhead). *The 3-D visualization of the nerve-vessel relationship was consistent with the intraoperative trajectory and findings* (D). D, *operative photograph showing the root entry zone of the right trigeminal nerve compressed by the rostral branch of the left superior cerebellar artery* (empty arrowhead), *consistent with operative simulation images* (B *and* C). *3-D magnetic resonance cisternogram* (E) *and fusion 3-D magnetic resonance cisternogram/angiogram* (F) *project superiorly (bird's-eye view) and show the spatial architecture of the left superior cerebellar artery and its tributaries. The entire 3-D shape of the right trigeminal nerve within the cistern from the orifice of Meckel's cave to the rootlet at the brainstem was depicted.* 3-D, *three-dimensional;* AICA, *anterior inferior cerebellar artery;* BA, *basilar artery;* CN-V, *Cranial Nerve V;* CN-VI, *Cranial Nerve VI;* CN-VII, *Cranial Nerve VII;* CN-VIII, *Cranial Nerve VIII;* OP, *operative photograph;* Meckel, *Meckel's cave;* MRC-MinIP, *magnetic resonance cisternogram minimum intensity projection;* MRC, *magnetic resonance cisternogram;* SCA, *superior cerebellar artery;* SCA-c, *superior cerebellar artery, caudal branches;* SCA-r, *superior cerebellar artery, rostral branches.*

vessel structures around the trigeminal nerve REZ, it may sometimes be difficult to infer a precise understanding of the 3-D architecture by the simple imaginary assessment based on reviewing one or more source images displayed in two-dimensional fashion. It may be easier to discern the relationships of the nerve-vessel complex at the trigeminal nerve REZ with 3-D displays. With the recent progress in computer medical visualization software (1, 17, 21–24), the 3-D reconstruction of images from the volumetric data of MRI, computed tomography, and digital angiography is feasibly performed in a short time. The 3-D magnetic resonance cisternogram, rendered with a perspective volume-rendering algorithm, can be reconstructed by selecting the information regarding the entire area with lower signal intensity than cerebrospinal fluid from the whole volume-rendering data set without targeting or trimming of the region of interest. In addition, the transparent imaging technique (21, 23) allows boundary imaging of the 3-D magnetic resonance cisternogram. Contours of the intra- and juxtacisternal objects are sharply represented as a series of rings, and the underlying structures can be visual-

ized directly through the space of rings from the outside to the inside the objects. Consequently, the 3-D magnetic resonance cisternogram represents a spatial relationship of the complicated anatomic elements within a cerebellopontine angle cistern, including the trigeminal nerve, offending vessels, and surrounding brainstem.

Fusion 3-D Magnetic Resonance Cisternogram/Angiogram for Operative Simulation

In this study, we used a boundary fusion imaging technique of the 3-D magnetic resonance cisternogram/angiogram (22–24), reconstructed by compositing the black blood 3-D magnetic resonance cisternogram and co-registered bright blood 3-D MRA in a single 3-D image, and applied it for the virtual reality of the preoperative assessment and surgical simulation of MVD in patients with ITN. With a boundary fusion image, the vascular components depicted on the 3-D magnetic resonance cisternogram (rendered as a series of rings in blue) can be discriminated from the complicated intra- and juxtacisternal nerve-vessel structures by referencing the overlapped 3-D MRA (rendered in red). Consequently, the boundary fusion 3-D magnetic resonance cisternogram/angiogram can provide a 3-D visualization of the actual contact between the offending vessels and the trigeminal nerve at the REZ. The presence of offending vessels and the compressive site of neurovascular conflict could be preoperatively assessed from the various viewpoints within the cistern and presumed by the preoperative simulation through the surgical access (surgeon's-eye view). Additionally, the blinded surgical trajectory could be discerned by the virtual image through the opposite direction projected from above (bird's-eye view) or transparently through the foreground objects.

Because retraction of the petrosal surface of the cerebellum and dissection of the arachnoid membranes are usually performed during surgical manipulation, the preoperative 3-D visualization of the nerve-vessel relationship without surgical intervention may not be identical to the operative fields, but the shape and spatial relationship of nerve-vessel structures are correlated well with the intraoperative trajectory and findings. The displacement of the anatomic elements within and adjacent to the cistern following surgical exposure always compromises a comparison of the pre- and intraoperative studies (21–24). In the present study, the offending vessels predicted by the preoperative images were consistent with the intraoperative field in most cases. In one missing case (Patient 7), the offending vessels predicted both a tributary of SPV and the rostral branch of SCA on the preoperative 3-D images. We found the contact of the trigeminal nerve with SCA, but not with SPV at the time of MVD surgery, probably because surgical dissection and suction of cerebrospinal fluid might displace the vein from the nerve at its ventral surface.

The virtual reality of the surgical simulation with the dynamic animation display of 3-D images provides realistic depiction and further understanding of the spatial anatomic relationship of the neurovascular compression. Consequently, fusion imaging allows the surgeon to look around the trigeminal nerve, to examine its ventral surface, and to trace its vascular anatomy, which may be obscured from view during MVD surgery.

Benefits and Limitations of the Boundary Fusion 3-D Magnetic Resonance Cisternogram/Angiogram

The boundary fusion image of the 3-D magnetic resonance cisternogram/angiogram can be a reference point that is useful to recognize and identify each anatomic element within the cisternal space allowing the surgeon to determine whether or not a structure is a vessel. The composition of a boundary image of the 3-D magnetic resonance cisternogram and a simple 3-D MRA is one of the best 3-D visualization to differentiate the vessels from the nerves and brainstem. The boundary imaging allows clear depiction of the contours of the foreground anatomic elements as a series of sharp rings or zebra stripes (in blue), so that the underlying vessels (in red) are visualized directly through the spaces between rings. In addition, fusion 3-D magnetic resonance cisternogram/angiogram may provide both information of the vascular morphology (in blue) (T2 FSE cisternogram) and intravascular flow condition (in red) (TOF, SPGR angiogram) composed in a single 3-D image.

Dynamic analyses of the images of 3-D MRA, 3-D MR cisternogram, and fusion 3-D magnetic resonance cisternogram/angiogram are necessary to trace the vessels back to a trunk artery of the basilar artery and VA or to large veins of SPV and superior petrosal sinus and also to trace the trigeminal nerve from Meckel's cave to the nerve rootlet at the brainstem. We can decide which are arteries, veins, and nerves on the 3-D magnetic resonance cisternogram. We can then reconstruct the static simulation images and animated images for the virtual reality of surgical access; those are not identical, but they are consistent, with the actual operative trajectory and fields.

The boundary fusion images may provide helpful information regarding the neurovascular conflict at the time of the MVD surgery. When utilizing the 3-D fusion imaging technique as a decision-making tool for MVD surgery, caution should used when deciding the significance or severity of neurovascular contact. In the absence of deep grooving or gross distortion of the nerve, it does not seem possible that this type of imaging technique can distinguish the significance of any particular contact between nerve and vessel. With further improvements in the computer medical visualization software and the quality of the source volumetric data, the 3-D fusion imaging technique may become a powerful tool in the planning and performance of MVD in patients with ITN.

Significance of Findings with Fusion 3-D Magnetic Resonance Cisternogram/Angiogram

The fusion imaging of the 3-D magnetic resonance cisternogram/angiogram may prove a useful adjunct for the diagnosis and decision-making process to execute the MVD in patients with ITN. However, the significance of the fusion 3-D magnetic resonance cisternogram/angiogram findings is yet to be determined. In patients with ITN or atypical facial pain, the magnetic resonance evidence for neurovascular contact is

observed not only in the symptomatic side, but also in the asymptomatic side (2). The significance of the fusion magnetic resonance findings of vascular contact with the trigeminal nerve needs to be clarified; the pathological neurovascular conflict needs to be differentiated from the non-pathological or innocent contact. It may be necessary to elucidate the more precise visualization of the compressive site and degree of the offending vessels to the affected trigeminal nerve, in conjunction with fine arterioles, perforators, and small venules around the trigeminal nerve REZ. Moreover, a few patients with symptomatic ITN may not exhibit evidence of neurovascular contact (10, 13) but may display a distortion of the trigeminal nerve or adhesive arachnoiditis at the rootlet of the trigeminal nerve. Because the fusion imaging of 3-D magnetic resonance cisternogram/angiogram can depict the spatial architecture of the intracisternal anatomic elements, including the nerve-vessel relationship, the morphology of the entire course of the intracisternal trigeminal nerve from Meckel's cave to the rootlet at the brainstem can be represented. Assessment of the nature of ITN and atypical facial pain (4) may be possible with use of fusion imaging. More work is required to validate the imaging technique and clarify the significance of MR findings regarding the pathological neurovascular conflict for the execution of the MVD in patients with ITN.

CONCLUSION

The fusion imaging of the 3-D magnetic resonance cisternogram and co-registered 3-D MRA may be useful in the preoperative assessment of MVD for ITN. The complex nerve-vessel structures at the trigeminal nerve REZ can be visualized in a 3-D fashion. The relationship of the offending vessels to the trigeminal nerve at the REZ may be discerned preoperatively from various viewpoints in the cerebellopontine angle cistern and through the simulated surgical access (surgeon's-eye view). The blinded surgical trajectory was discerned by the virtual image through the opposite direction projected from above (bird's-eye view). With a fusion 3-D magnetic resonance cisternogram/angiogram, the 3-D visualization of the nerve-vessel relationship was consistent with the intraoperative trajectory and findings. A fusion imaging technique of 3-D magnetic resonance cisternogram/angiogram can be applied to investigate other neurovascular compressive syndromes, including hemifacial spasm (15–17, 20), glossopharyngeal neuralgia (8, 17), vestibulocochlear compressive tinnitus, hearing loss (7, 17, 20), and neurogenic hypertension (6, 17).

REFERENCES

1. Akimoto H, Nagaoka T, Nariai T, Takada Y, Ohno K, Yoshino N: Preoperative evaluation of neurovascular compression in patients with trigeminal neuralgia by use of three-dimensional reconstruction from two types of high-resolution magnetic resonance imaging. **Neurosurgery** 51:956–962, 2002.
2. Anderson VC, Berryhill PC, Sandquist MA, Ciaverella DP, Nesbit GM, Burchiel KJ: High-resolution three-dimensional magnetic resonance angiography and three-dimensional spoiled gradient-recalled imaging in the evaluation of neurovascular compression in patients with trigeminal neuralgia: A double-blind pilot study. **Neurosurgery** 58:666–673, 2006.
3. Boecher-Schwarz HG, Bruehl K, Kessel G, Guenthner M, Perneczky A, Stoeter P: Sensitivity and specificity of MRA in the diagnosis of neurovascular compression in patients with trigeminal neuralgia. A correlation of MRA and surgical findings. **Neuroradiology** 40:88–95, 1998.
4. Burchiel KJ: A new classification for facial pain. **Neurosurgery** 53: 1164–1167, 2003.
5. Chávez G, De Salles AA, Solberg TD, Pedroso A, Espinoza D, Villablanca P: Three-dimensional fast imaging employing steady-state acquisition magnetic resonance imaging for stereotactic radiosurgery of trigeminal neuralgia. **Neurosurgery** 56:E628, 2005.
6. Colón GP, Quint DJ, Dickinson LD, Brunberg JA, Jamerson KA, Hoff JT, Ross DA: Magnetic resonance evaluation of ventrolateral medullary compression in essential hypertension. **J Neurosurg** 88:226–231, 1998.
7. De Ridder D, Ryu H, Møller AR, Nowé V, van de Heyning P, Verlooy J: Functional anatomy of the human cochlear nerve and its role in microvascular decompressions for tinnitus. **Neurosurgery** 54:381–390, 2004.
8. Fischbach F, Lehmann TN, Ricke J, Bruhn H: Vascular compression in glossopharyngeal neuralgia: Demonstration by high-resolution MRI at 3 Tesla. **Neuroradiology** 45:810–811, 2003.
9. Hitotsumatsu T, Matsushima T, Inoue T: Microvascular decompression for treatment of trigeminal neuralgia, hemifacial spasm, and glossopharyngeal neuralgia: Three surgical approach variations: Technical note. **Neurosurgery** 53:1436–1443, 2003.
10. Ishikawa M, Nishi S, Aoki T, Takase T, Wada E, Ohwaki H, Katsuki T, Fukuda H: Operative findings in cases of trigeminal neuralgia without vascular compression: Proposal of a different mechanism. **J Clin Neurosci** 9:200–204, 2002.
11. Jäger HR, Ellamushi H, Moore EA, Grieve JP, Kitchen ND, Taylor WJ: Contrast-enhanced MR angiography of intracranial giant aneurysms. **AJNR Am J Neuroradiol** 21:1900–1907, 2000.
12. Jannetta PJ: Observations on the etiology of trigeminal neuralgia, hemifacial spasm, acoustic nerve dysfunction and glossopharyngeal neuralgia: Definitive microsurgical treatment and results in 117 patients. **Neurochirurgia** 20:145–154, 1977.
13. Kondo A: Follow-up results of microvascular decompression in trigeminal neuralgia and hemifacial spasm. **Neurosurgery** 40:46–52, 1997.
14. Mamata Y, Muro I, Matsumae M, Komiya T, Toyama H, Tsugane R, Sato O: Magnetic resonance cisternography for visualization of intracisternal fine structures. **J Neurosurg** 88:670–678, 1998.
15. Mitsuoka H, Tsunoda A, Okuda O, Sato K, Makita J: Delineation of small nerves and blood vessels with three-dimensional fast spin-echo MR imaging: Comparison of presurgical and surgical findings in patients with hemifacial spasm. **AJNR Am J Neuroradiol** 19:1823–1829, 1998.
16. Naganawa S, Koshikawa T, Fukatsu H, Ishigaki T, Fukuta T: MR cisternography of the cerebellopontine angle: Comparison of three-dimensional fast asymmetrical spin-echo and three-dimensional constructive interference in the steady-state sequences. **AJNR Am J Neuroradiol** 22:1179–1185, 2001.
17. Naraghi R, Hastreiter P, Tomandl B, Bonk A, Huk W, Fahlbusch R: Three-dimensional visualization of neurovascular relationships in the posterior fossa: Technique and clinical application. **J Neurosurg** 100:1025–1035, 2004.
18. Rhoton AL Jr: The cerebellopontine angle and posterior fossa cranial nerves by the retrosigmoid approach. **Neurosurgery** 47 [Suppl 3]:S93–S129, 2000.
19. Rubinstein D, Sandberg EJ, Breeze RE, Sheppard SK, Perkins TG, Cajade-Law AG, Simon JH: T2-weighted three-dimensional turbo spin-echo MR of intracranial aneurysms. **AJNR Am J Neuroradiol** 18:1939–1943, 1997.
20. Ryu H, Tanaka T, Yamamoto S, Uemura K, Takehara Y, Isoda H: Magnetic resonance cisternography used to determine precise topography of the facial nerve and three components of the eighth cranial nerve in the internal auditory canal and cerebellopontine angle cistern. **J Neurosurg** 90:624–634, 1999
21. Satoh T, Onoda K, Tsuchimoto S: Visualization of intraaneurysmal flow patterns with transluminal flow images of 3-D MR angiograms in conjunction with aneurysmal configurations. **AJNR Am J Neuroradiol** 24:1436–1445, 2003.
22. Satoh T, Omi M, Ohsako C, Fujiwara K, Tsuno K, Sasahara W, Onoda K, Tokunaga K, Sugiu K, Date I: Differential diagnosis of the infundibular dilation and aneurysm of internal carotid artery: Assessment with fusion imaging of 3-D MR cisternography/ angiography. **AJNR Am J Neuroradiol** 27:306–312, 2006.

23. Satoh T, Omi M, Ohsako C, Katsumata A, Yoshimoto Y, Tsuchimoto S, Onoda K, Tokunaga K, Sugiu K, Date I: Visualization of aneurysmal contours and perianeurysmal environment with conventional and transparent 3-D MR cisternography. **AJNR Am J Neuroradiol** 26:313–318, 2005.
24. Satoh T, Omi M, Ohsako C, Katsumata A, Yoshimoto Y, Tsuchimoto S, Onoda K, Tokunaga K, Sugiu K, Date I: Influence of perianeurysmal environment on the deformation and bleb formation of the unruptured cerebral aneurysm: Assessment with fusion imaging of 3-D MR cisternography and 3-D MR angiography. **AJNR Am J Neuroradiol** 26:2010–2018, 2005.
25. Sindou M, Howeidy T, Acevedo G: Anatomical observations during microvascular decompression for idiopathic trigeminal neuralgia (with correlation between topography of pain and site of neurovascular conflict). Prospective study in a series of 579 patients. **Acta Neurochir (Wien)** 144:1–13, 2002.
26. Tsuchiya K, Aoki C, Hachiya J: Evaluation of MR cisternography of the cerebellopontine angle using a balanced fast-field-echo sequence: Preliminary findings. **Eur Radiol** 14: 239–242, 2004.
27. Yoshino N, Akimoto H, Yamada I, Nagaoka T, Tetsumura A, Kurabayashi T, Honda E, Nakamura S, Sasaki T: Trigeminal neuralgia: Evaluation of neuralgic manifestation and site of neurovascular compression with 3-D CISS MR imaging and MR angiography. **Radiology** 228:539–545, 2003.
28. Yousry I, Moriggl B, Holtmannspoetter M, Schmid UD, Naidich TP, Yousry TA: Detailed anatomy of the motor and sensory roots of the trigeminal nerve and their neurovascular relationships: A magnetic resonance imaging study. **J Neurosurg** 101:427–434, 2004.

Acknowledgments

We thank Megumi Omi, Radiological Technologist, Chika Ohsako and Mutsue Nabeshima, Clinical Technologists, Ryofukai Satoh Neurosurgical Hospital, for technical assistance in conducting magnetic resonance studies. Presented in part at the 64th Annual Meeting of Japan Neurosurgical Society, October 5–7, 2005, Yokohama, Japan, and at the 29th Annual Meeting of the Japan Society for Central Nervous System Computed Imaging, January 27–28, 2006, Tokyo, Japan.

COMMENTS

Many treatment strategies are available for trigeminal neuralgia. Radiosurgery is a new tool proposed as a minimally invasive therapy. Nevertheless, the published data and our own experience demonstrate that this is a lesional procedure with a success rate as high as percutaneous methods. Microvascular decompression (i.e., resolution of the vascular compression between nerve and vessels) remains the etiological therapy with the best chance of success without trigeminal sensory deficit. Our experience, which is based on more than 600 cases with a follow-up period of at least 4 years, concurs with the published results that demonstrate a long-term success rate of more than 80% (i.e., these patients were pain free without any medication and without any neurological deficits, such as trigeminal sensory and motor deficit). The main problem in surgery is indication and selection of patients, especially when different treatments are available. Particularly for trigeminal neuralgia, the need for suggesting percutaneous methods, open surgery, or radiosurgery is filled with professional and medicolegal challenges. The authors of this article should be complimented for providing the neurosurgical community with an opportunity to image the vascular relationships of the trigeminal nerve. After reading this article, case selection should be improved in the general population of patients affected by facial pain and typical or atypical neuralgia. This method should be used to screen candidates for lesional procedures (i.e., radiosurgery or percutaneous methods) to prevent patients with clear evidence of nerve compression from experiencing nerve damage when microvascular decompression is performed. Our experience suggests that the fate of patients with clear nerve compression who undergo lesional procedures is pain recurrence, repeated lesional procedures, and, at the end, annoying and painful, if not dehibilitating, dysesthesia. In addition, the possibility of double pathology in patients with multiple sclerosis should not be forgotten, as this method of imaging can benefit the decision-making process. Patients with recurrent pain would also benefit from this kind of preoperative imaging, which verifies the new etiology of the disease, and this, in our opinion, is the major merit of the article.

Paolo Ferroli
Giovanni Broggi
Milan, Italy

The authors have applied a fusion imaging technique of three-dimensional (3-D) magnetic resonance cisternography and co-registered 3-D magnetic resonance angiography that offered virtual reality for the preoperative simulation of the neurovascular contact with the trigeminal nerve at the root entry zone. It is an interesting technique that will be advanced further in the future. At the present time, it shows relationships between the structures but does not provide a way to quantify the degree of neurovascular conflict to diagnose neurovascular conflict or to distinguish between symptomatic and innocent conflict. Therefore, I am not yet comfortable making decisions about surgical indications based upon this technique.

Nevertheless, it is an interesting technique that is worthwhile for surgeons to help visualize the operative field before surgery. I have always thought that surgery is performed better when the surgeon has an excellent 3-D view in his or her mind before the procedure and during the exposure.

Thomas Naidich
Neuroradiologist
Kalmon D. Post
New York, New York

The authors present an interesting method of using various magnetic resonance imaging (MRI) sequences to perform a 3-D reconstruction of the complex anatomy of the cerebellopontine angle. This 3-D reconstruction aids the surgeon when planning surgery for microvascular decompression of the trigeminal nerve for trigeminal neuralgia. The authors use this method on a consecutive series of 12 patients and present their findings on the concordance of operative findings with the preoperatively obtained 3-D images. They conclude that their 3-D model accurately depicts the neurovascular relationships within the cerebellopontine angle, aiding the surgeon in the planning of the operation.

This is a well-written and documented article that demonstrates the utility of 3-D modeling in this setting. The ability to "see" what is going on in the cerebellopontine angle has been elusive, and microvascular decompressions are frequently exploratory surgeries in which the surgeon knows little about what vascular structures may or may not be contacting the trigeminal nerve. With the advent of high-resolution imaging, such as MRI, we have gotten a glimpse into the microanatomy of this region, but the interpretation of two-dimensional images leaves much to be desired. Using 3-D modeling based on several types of image sequences, we are now able to obtain a better picture of the neurovascular relationships.

Although the use of 3-D rendering of MRI scans is an exciting development in the preoperative planning of these cases, the images presented also point out some of the weaknesses of this method. First, the images presented by the author, which likely represent the clearest examples in their series, are difficult to interpret. Without the numerous annotations, I would have difficulty identifying the various structures. This probably results from the fact that these are static images, whereas the rendering software provides the clinician with dynamic

images that can be manipulated to identify various structures. Secondly, I don't think it is feasible to detect the "significance" of the neurovascular contact or its "degree" with this type of image analysis. In the absence of deep grooving or gross distortion of the nerve, it does not seem possible for this type of technique to distinguish the significance of any particular contact between nerve and vessel. Rather, I think the strength of this tool is in its ability to allow the surgeon to look around the nerve, to examine its ventral surface, and to trace vascular anatomy, which may be obscured from view during surgery. With improvements in the software and the quality of the source images, this may become a powerful tool in the planning and performance of microvascular decompressions.

Oren Sagher
Ann Arbor, Michigan

The authors describe an imaging technique of 3-D magnetic resonance cisternography and coregistered 3-D magnetic resonance angiography that allows virtual reality for the preoperative simulation of the neurovascular conflict at the trigeminal nerve root entry zone. In a consecutive series of 12 patients with idiopathic trigeminal neuralgia, they found preoperative vascular contact in all 12 patients, both by imaging and by direct intraoperative observation. Preoperative imaging showed trigeminal nerve contact with the superior cerebellar artery (SCA) in 10 patient, SCA and venous contact in two patients, anterior inferior cerebellar artery contact in one patient, and posterior inferior cerebellar artery/vertebral artery contact in one patient. At surgery, identical findings were noted in all patients, except one in whom only SCA (and no venous) contact was found.

Preoperative assessment of the neurovascular contact is important, and improved methodology is welcome. However, there are some limitations in the present study. Those who evaluated the preoperative images were the people who performed the surgery and reported on the intraoperative findings. Their awareness of one set of findings may have influenced their impression of the other findings. Although all operated patients had neurovascular contacts, it is not clear how many patients with idiopathic trigeminal neuralgia did not have such contacts and were not operated. Other series have found more cases of venous contact than described here. It will require more patients studied by these and other observers before the exact role of the new fusion technique is established.

Ronald Brisman
New York, New York

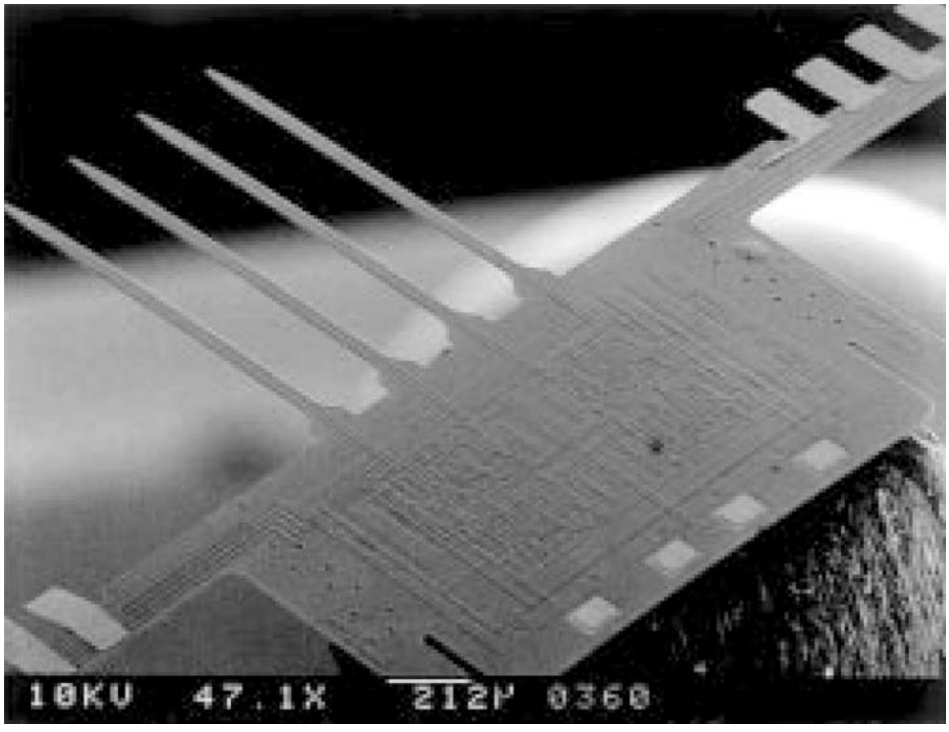

Invasive neural prosthesis. Scanning electron microscopy of neural microelectrode array (MEA) probes and recording on-chip signal processors. (Bai Q, Wise KD: Single-unit neural recording with active microelectrode arrays. **IEEE Trans Biomed Eng** 48:911–920, 2001.) Please see additional material on pages 88, 96, and 128.